Research Updates: Epitaxial strain relaxation and associated interfacial reconstructions: The driving force for creating new structures with integrated functionality

Yuanyuan Zhu, Aiping Chen, Honghui Zhou, Wenrui Zhang, Jagdish Narayan, Judith L. MacManus-Driscoll, Quanxi Jia, and Haiyan Wang

Research Updates: Epitaxial strain relaxation and associated interfacial reconstructions: The driving force for creating new structures with integrated functionality

Yuanyuan Zhu,[1] Aiping Chen,[2] Honghui Zhou,[3] Wenrui Zhang,[1]
Jagdish Narayan,[3] Judith L. MacManus-Driscoll,[4] Quanxi Jia,[5]
and Haiyan Wang[1,2,a]

[1]*Program of Materials Science and Engineering, Texas A&M University, College Station, Texas 77843, USA*
[2]*Department of Electrical and Computer Engineering, Texas A&M University, College Station, Texas 77843, USA*
[3]*Department of Materials Science and Engineering, NSF Center for Advanced Materials and Smart Structures, North Carolina State University, Raleigh, North Carolina 27695, USA*
[4]*Department of Materials Science and Metallurgy, University of Cambridge, Pembroke Street, Cambridge CB2 3QZ, United Kingdom*
[5]*Center for Integrated Nanotechnologies (CINT), Los Alamos National Laboratory, Los Alamos, New Mexico 87545, USA*

Here, we report detailed strain mapping analysis at heterointerfaces of a new multi-ferroic complex oxide $Bi_3Fe_2Mn_2O_x$(BFMO322) supercell and related layered structures. The state-of-the-art aberration corrected scanning transmission electron microscopy (Cs-corrected STEM) and the modified geometric phase analysis (GPA) have been used to characterize the self-assembled transitional layers, misfit defects, and, in particular, the biaxial lattice strain distributions. We found that not only a sufficient lattice misfit is required through substrate selection and to be preserved in initial coherent epilayer growth, but also an appropriate interfacial reconstruction is crucial for triggering the growth of the new BFMO322 supercell structure. The observation of new transitional interfacial phases behaving like coherent film layers within the critical thickness challenges the conventional understanding in existing epitaxial growth model. © *2013 Author(s). All article content, except where otherwise noted, is licensed under a Creative Commons Attribution 3.0 Unported License.*
[http://dx.doi.org/10.1063/1.4828936]

Perovskite oxides exhibit very rich physical properties including high-temperature superconductivity,[1] magnetoresistance,[2,3] multiferroics,[4] and many others. These fascinating physical behaviors are strongly related to the couplings between spin, charge, lattice, and orbital degrees of freedom of the material. Many of these properties are directly related to the strain state of the oxide films.[5,6] During the epitaxial growth of oxide thin films, biaxial lattice strain can be automatically generated due to film-substrate lattice mismatch, and therefore can be controlled by substrate selection. It plays a vital role in tailoring the functionalities of perovskite thin films such as optical, electrical, and magnetic properties, and understanding the epitaxial strain relaxation in oxide thin film is thus highly crucial for controlling the properties of perovskite oxide thin films.

In conventional heteroepitaxy growth, lattice strain f, arising from the lattice mismatch between the film and the substrate, is given by $f = 2(a_f - a_s)/(a_f + a_s)$. a_f and a_s are the unstrained lattice parameters of the film and the substrate, respectively. In lattice-matching epitaxy, where the lattice misfit is small ($f < 1\%$), films grow pseudomorphically up to a critical thickness (h_c) where it becomes energetically favorable for the film to generate misfit dislocations. When the misfit strain f

---

[a]Author to whom correspondence should be addressed. Electronic mail: wangh@ece.tamu.edu. Tel.: +1 9798455082. Fax: +1 9798456259.

1, 050702-1

is larger ($f > 7\%$), domain matching epitaxy (DME) takes place. In this framework, the conventional lattice-matching epitaxy becomes a special case where the epitaxial growth of thin films is possible by matching of domains where integral multiples of major lattice planes match across the interface. Narayan and co-workers reported the DME growth of TiN/Si (100) with 3/4 matching, the AlN/Si (100) with 4/5 matching, and the ZnO/α-Al$_2$O$_3$ (0001) with 6/7 matching of major planes across the film/substrate interface.[7, 8]

The growth of epitaxial thin film is strongly governed by free energy of the system. Formation of misfit dislocations is a well-accepted mechanism to release the strain energy in epitaxial system with a large lattice mismatch. However, besides misfit dislocation formation, other phenomena including lattice distortion,[9] formation of buffer layer,[10, 11] and even new phases[12] have also been reported in oxide films for strain relaxation. Zhou *et al.* reported a thin interlayer formed between a VO$_2$ film and a sapphire substrate.[11] The thin layer can minimize the interface free-energy and accommodate the symmetry mismatch between the substrate and the film. Chen *et al.* demonstrated the formation of a brand-new bismuth-based supercell structure as another means of strain relaxation.[12] It shows the possibility of integrating functional oxides with different magnetic/electronic properties into layered structures that exhibit various responses simultaneously.[13] The formation of this multiferroic Bi$_3$Fe$_2$Mn$_2$O$_x$(BFMO322) supercell, with a cation ratio of Bi:Fe:Mn = 3:2:2, was found to exist greatly depending on substrate selection. Under identical deposition condition, films directly grown on SrTiO$_3$(STO) single-crystalline substrates give the conventional pseudo-perovskite Bi$_2$FeMnO$_6$ structure;[14] while the BFMO322 supercell structure has been established on LaAlO$_3$(LAO) substrates with a much pronounced lattice misfit (ca. -2.0%, comparing with that of on STO ca. -0.6%).[12]

The formation of new phases beyond h_c, as a possibly new strain relaxation mechanism, is an open question. It could exist in many other oxide systems and lead to many exciting new phases and new functionalities. Understanding the underlying mechanism for the new phase formation is therefore critical for the above new phase exploration. In this work, we have investigated the strain relaxation mechanism(s) in the novel bismuth-based supercell structure by conducting atomic structure investigations at the heterogeneous interfaces. For comparison, three heterosystems were studied: (1) the pseudo-perovskite Bi$_2$FeMnO$_6$/STO; (2) the new BFMO322/LAO in [010] and [100] zone axis, respectively; and (3) the tilted pseudo-perovskite Bi$_2$FeMnO$_6$/LAO. To understand what triggers the new supercell structure, important heterointerface structures such as interfacial contact, self-assembled interlayers, and misfit dislocations were characterized using aberration corrected scanning transmission electron microscopy (Cs-corrected STEM) at atomic scale. In particular, epitaxial lattice strain has been quantified within 1 nm spatial resolution across each heterointerface using an optimized geometric phase analysis (GPA).[15]

The deposition of epitaxial BFMO films was conducted by a standard pulsed-laser deposition (PLD) technique (KrF excimer laser $\lambda = 248$ nm) on single crystalline LAO (001) and STO (001) substrates. A composite target with a 1:1 molar ratio of Bi$_{1.05}$FeO$_3$ and Bi$_{1.05}$ MnO$_3$ was prepared through a conventional ceramic sintering process. In this work, we focused on the BFMO films, up to a thickness of approximately 40 nm, grown under optimum PLD conditions for high purity layered BFMO phase at a growth temperature of 700 °C and a laser pulse rate of 2 Hz. The details on deposition parameter optimization and film post annealing can be found elsewhere.[12]

Cross-sectional specimens of the heterointerfaces were prepared through a conventional TEM sample preparation routine along ⟨100⟩ direction. Starting with cutting and gluing, the TEM specimens were then ground, planar parallel polished, and further thinned in the center by dimpling. Ar ion milling was used to obtain a perforation and electron transparent thin area with a Gatan Precision Ion Polishing System (Gatan, Pleasanton, California). TEAM0.5,[16] a modified FEI Titan microscope equipped with a special high-brightness Schottky-field emission electron source as well as two improved hexapole-type spherical aberration correctors was employed. One of main advantages of the Cs-corrected STEM is a significant improvement in spatial resolution, which has been demonstrated to be as high as 0.5 Å in TEAM0.5.[17] All high angle annular dark-field (HAADF) STEM micrographs in this paper were recorded with a convergence semi-angle of 17 mrad after fine-tuning of the probe corrector at 300 kV to a flat-phase angle of over 25 mrad,[18] and with a ADF detector inner semi-angle of 68 mrad. To extract the actual biaxial strain field at heterointerfaces,
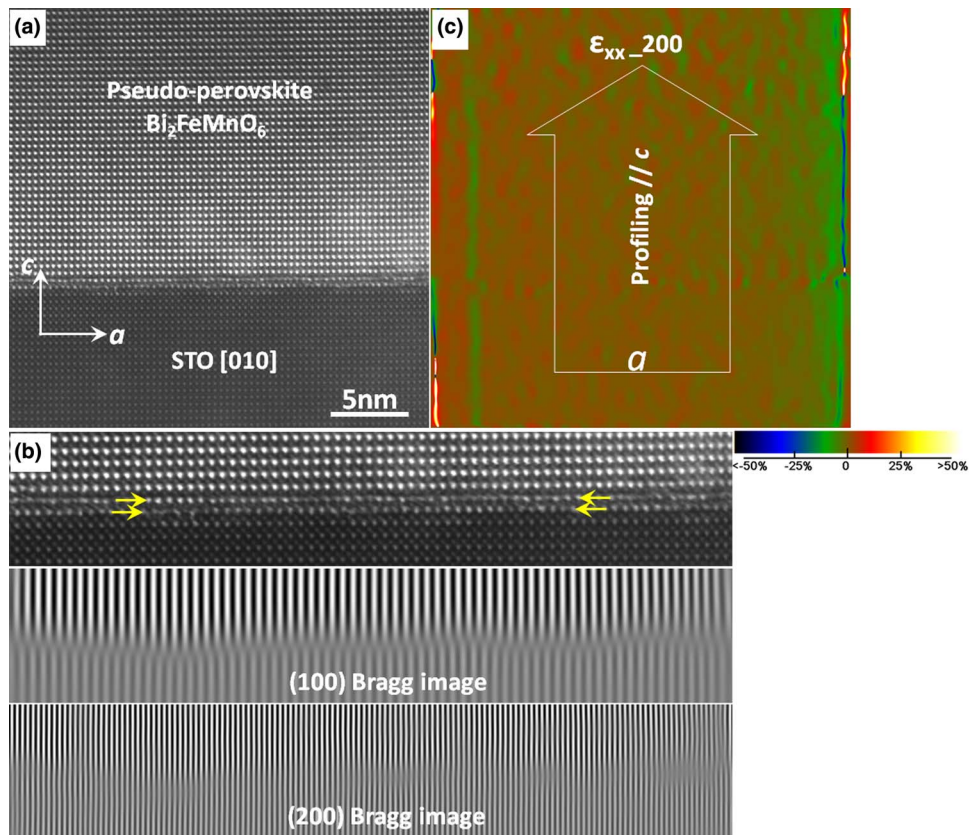
FIG. 1. (a) A representative cross-sectional STEM image of the 40 nm-thick Bi_2FeMnO_6 epitaxial thin film on STO (100) in the $\langle 100 \rangle$ zone axis. (b) Enlarged interface region in (a) and corresponding (100) and (200) Bragg images. (c) The GPA biaxial strain map ε_{xx} of (a). It was calculated using both (200) and (002) Bragg vectors. Note that the stacking fault at the interface does not introduce any additional extra-half inset.

a modified GPA was applied to the obtained Cs-corrected STEM images. This STEM-based GPA strain profile has been proven being able to achieve high accuracy in the STEM fast-scan direction with a spatial resolution less than 1 nm. Details on the optimized GPA can be found elsewhere.[15] Since we focus on biaxial strain in this work, the accuracy estimated from STEM images of substrate lattice for the in-plane strain ε_{xx} is within 0.10% (for details, please see Fig. S1 of the supplementary material).[19] A scale range of -50% to $+50\%$ was applied to all strain maps here for consistency.

Figure 1(a) is a representative cross-sectional HAADF-STEM (Z-contrast) image of the heterointerface of the pseudo-perovskite Bi_2FeMnO_6/STO. In the Z-contrast image, the Bi_2FeMnO_6 film shows a brighter contrast than the STO substrate due to a higher average atomic number. In the enlarged interface region in Fig. 1(b), in the STO substrate, the Sr-columns appear as the brighter dots with the less bright TiO-columns located at the centers of the Sr-square lattice, presenting a standard perovskite lattice in $\langle 100 \rangle$ projection. Similarly, in the film, Bi-columns appear as the brightest square lattice with FeO/MnO-columns at their centers. Although the upper film region presents a single-crystal-like quality, as shown by the arrows and corresponding Bragg filtered images in Fig. 1(b), an in-plane lattice modification was found in the Bi_2FeMnO_6 film initial plane. To explore the effects of the interfacial defects on film biaxial strain, we applied the optimized GPA[15] and the in-plane lattice strain map ε_{xx} (a-lattice displacement) is presented in Fig. 1(c). This strain map, essentially with a color contour, provides a direct illustration of local lattice displacement from a reference crystal,[20] where in this case the STO substrate (i.e., the ε_{xx} of STO is zero). For details on STEM-based GPA processing please refer to the previous work.[15] It is interesting to note that even with the presents of interfacial imperfections, the strain contour is in a relatively uniform color suggesting that there is no obvious strain variation across the heterointerface.
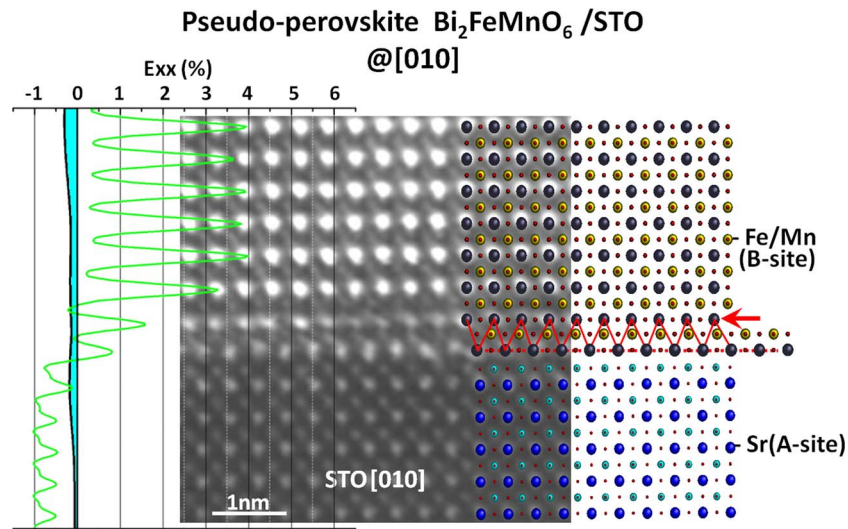
FIG. 2. Interfacial atomic contact and biaxial strain profile across the pseudo-perovskite Bi_2FeMnO_6/STO heterointerface. Atomic models of perovskite in $\langle 100 \rangle$ projection schematically illustrate the stacking fault at the interface. The STEM intensity profile across the LAO/STO interface was superimposed (in green) on the ε_{xx} profile for the illustration of the position of local lattice.

Further analysis of the interfacial atomic contact and the epitaxial strain distributions of the Bi_2FeMnO_6/STO are shown in Fig. 2. As denoted by a red arrow, a stacking fault emerges at the third monolayer of the film, i.e., the lattices above and the stacking fault are shifted relative to one another by a half unit cell. Then, the Sr-columns, occupying the A-site of the substrate perovskite structure ABO_3, vertically align with the Fe/Mn-columns of the B-site in the pseudo-perovskite Bi_2FeMnO_6 film. This nearly perfect half-*a* shifting explains that the (200) Bragg image in Fig. 1(b) is continuous but the (100) Bragg fringes are interrupted at the interface. However, the formation of the stacking fault does not influence the effect of the substrate-introduced epitaxial strain on the film. As shown in the strain profile coated in cyan in Fig. 2 (along the arrow in Fig. 1(c)), after crossing the heterointerface, the biaxial strain ε_{xx} (*a*-lattice displacement) is still close to zero (as in the STO substrate) in the first five-unit-cell-thick film region, and becomes slightly relaxed in the layers above. This indicates that, similar to a previous report,[14] the pseudo-perovskite Bi_2FeMnO_6 film remains strained (compressive) on STO substrates, even with the presence of the stacking fault observed here.

When applying pseudo-perovskite LAO (001) substrates, we obtained the multiferroic BFMO322 supercell. An overview of the BFMO322 film on LAO (001) is shown in Fig. 3(a), presenting distinctively bright Bi_2O_2 layers stacking in a highly epitaxial manner. We have identified that this commensurate supercell structure has different in-plane lattices *a* and *b*, as well as different lattice projections from $[010]_{pseudo-perovskite}$ ($[010]_p$) and from $[100]_p$ direction.[12] Cs-corrected STEM images were taken from both zone axes for interfacial analysis. The BFMO322/LAO in [010] and corresponding lattice strain map ε_{xx} are shown in Figs. 3(b) and 3(c), respectively. Compared to the strain map of heterostructures Bi_2FeMnO_6/STO (Fig. 1(c)), an obvious strain jump, color coded from brown to red, was observed across the interface of BFMO322/LAO. Corresponding (200) Bragg filtered image of the interface region reveals that there are stacking faults in the transition metal plane. Similar to what observed in another layered-structure of the superconducting $YBa_2Cu_3O_{7-\delta}$,[21] these stacking faults present a fifteen to sixteen (200)-plane matching, as enlarged in Fig. 3(d), contributing to partial edge dislocations with a spacing about 5 nm.

Moreover, a careful analysis in Fig. 4 shows that this abrupt strain relaxation occurred at about 4 nm above the LAO substrate terminating layer (marked by a white arrow). The crystal structure of the BFMO322 is under investigation; while the cation sublattice of the BFMO322 has been identified.[12] A ball model is demonstrated here in Fig. 4 near the [010] zone axis, showing a signature alternating
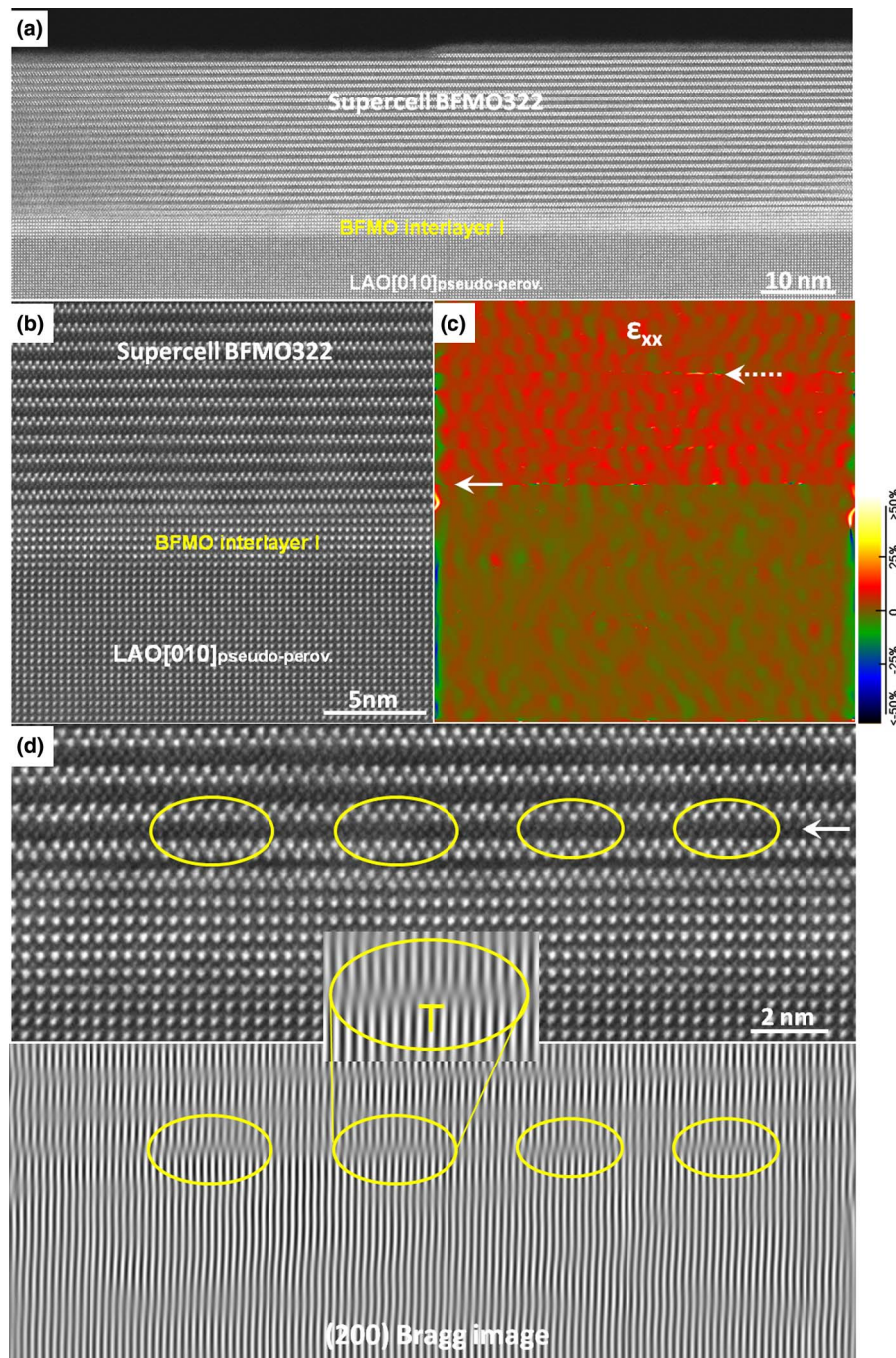
FIG. 3. (a) A cross-sectional STEM overview of the 36 nm-thick BFMO322/LAO in the [010] zone axis. (b) A representative Cs-corrected STEM image of the heterointerface of BFMO322/LAO in the [010]. (c) The corresponding GPA biaxial strain map ε_{xx}, calculated using both (200) and (002) Bragg vectors. A dashed arrow denotes the staking faults in the BFMO322 film. (d) Enlarged interface region in (a) and corresponding (200) Bragg images. The inset is to show a partial (200) inserting plane at the stacking fault.

Bi-column triangles. In between the top BFMO322 supercell film and the LAO substrate, there are actually two highly strained transition layers (interlayers I and II) with a thickness of h_{c1} and h_{c2}, respectively. Interlayer I was found exhibiting a higher degree of unit cell anisotropy of c/a = 1.15 than that of 1.02 for the pseudo-perovskite Bi_2FeMnO_6 on STO,[12] suggesting a greater
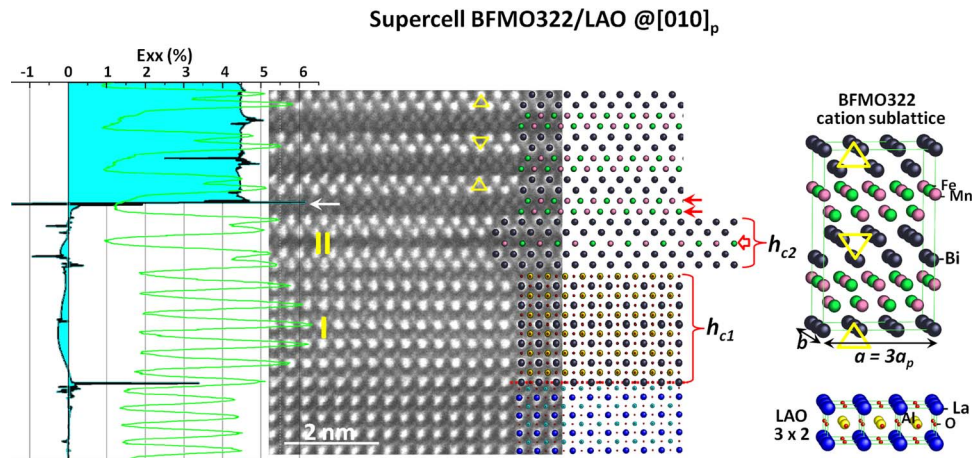
FIG. 4. Interfacial atomic contact and biaxial strain profile across the supercell BFMO322/LAO heterointerface in the [010]. The abrupt strain relaxation in the ε_{xx} profile is marked by a white arrow. Two transition layers are noted as "I" and "II," with a thickness of h_{c1} and h_{c2}, respectively. In addition, the STEM intensity profile (in green) across the interface was superimposed on the ε_{xx} profile for the illustration of the position of local lattice. Ball models of the BFMO 322 cation sublattice (1 unit-cell) and the LAO pseudo-perovskite (3 by 2 unit-cell) near the [010] projection are presented. The atomic arrangements of the Bi-column are marked by triangles. The neighboring Bi_2O_2 sheets are alternating (the same every other Bi_2O_2 sheets) in the [010] direction.

(absolute) biaxial strain. Formation of interlayer I is possibly related to the pseudomorphic growth on the single-crystalline substrate,[22] since it preserves the crystal structure of the pseudo-perovskite LAO substrate. Interlayer II, however, shares a similar triangle-stripe feature of the bright Bi_2O_2 layers as in the above BFMO322 supercell structure, but has only one Fe-O/Mn-O layer in between (pointed by an open arrow). In most view fields of this heterointerface of BFMO322/LAO in [010], interlayer II was found consisting of two Bi_2O_2 layers (bright dots), and in some regions it can have three Bi_2O_2 layers. The conversion of two Bi_2O_2 layers to three in interlayer II could be related to the formation of in-plane dislocation partials (for details please see Fig. S2 of the supplementary material).[19] Thus, it suggests that the crystal structure and very likely also the film stoichiometry gradually transfer from a highly distorted pseudo-perovskite one to the BFMO322 supercell through transitional regions I and II.

Since the formation mechanism of the new thin film phase of BFMO322 is the main topic of this work, we further examined its heterointerface structure by exploring the other in-plane crystallographic direction of $[100]_p$. A representative cross-sectional STEM image is presented in Fig. 5(a). Under this zone axis, localized dislocation-core-like contrasts were observed distributing approximately 10 nm apart along the interface of the interlayers and the BFMO322 supercell. As shown in the corresponding (020) Bragg filtered images in Fig. 5(b), unlike the stacking faults observed under [010] (Fig. 3(c)), these interfacial defects are complex dislocations with two (020) extra-half inserting planes. In fact, different partial dislocations have been demonstrated in perovskite films such as $Ba_{0.3}Sr_{0.7}TiO_3$[23] and $SrTiO_3$[24] on LAO. Nevertheless, these edge dislocation partials serve also as misfit defects to relax the compressive lattice strain in interlayer I, resulting in the strain jump at the supercell initiating layer as pointed by the white arrow in the GPA strain map in Fig. 5(c). Further interfacial contact analysis in Fig. 6 reveals that, although the interlayer I has the same thickness under both observation projections, the following interlayer in the view field (noted as the interlayer II' to distinguish from the interlayer II) is thinner than that of in Fig. 4. This slightly early relaxed biaxial strain in Fig. 6 indicates that the complex dislocations cores accompanying with greater interfacial reconstructions are likely to be more effective in strain relaxation than the stacking faults in Fig. 3(d).

To understand the substrate-dependent of the BFMO thin film phase formation, the biaxial strain ε_{xx} profiles from the above two heterostructure systems, i.e., the pseudo-perovskite Bi_2FeMnO_6/STO, and the supercell BFMO322/LAO in both [100] and [010] projections with interlayer II consisting
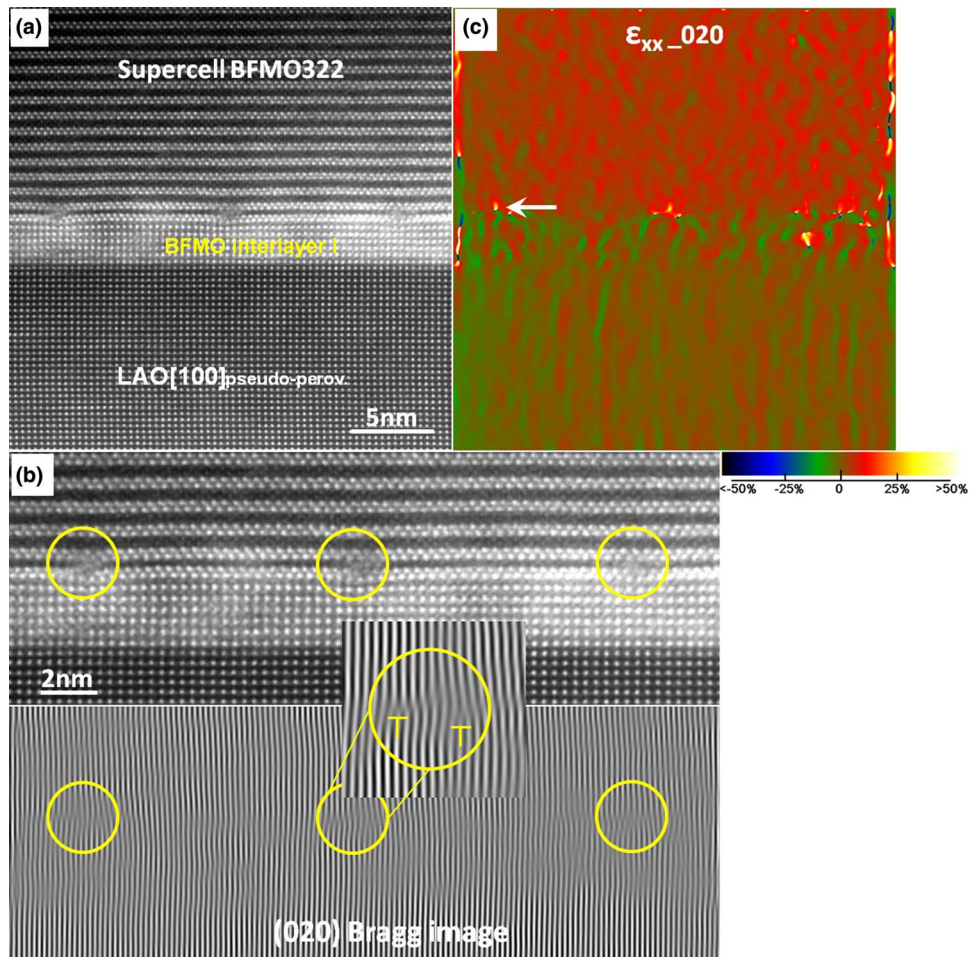
FIG. 5. (a) A representative cross-sectional STEM image of the 36 nm-thick BFMO322/LAO in the [100] zone axis. (b) Enlarged interface region in (a) and corresponding (020) Bragg images. Misfit dislocation cores are denoted, with spacing about 10 nm apart. The inset is a representative core region enlarged to show two partial (020) inserting planes. (c) The GPA biaxial strain map ε_{xx} of (a), showing a strain change across the interface.

of two and three Bi_2O_2 layers are summarized in Fig. 7. The mean ε_{xx} strain in the top epitaxial film region is calculated and denoted accordingly. It is obvious that the pseudo-perovskite Bi_2FeMnO_6 film is greatly confined by the STO substrate (with a relative strain of only -0.33%); whereas, the supercell BFMO322 film on LAO is (partially) relaxed to about 3.7%–4.4%. Most interesting is the strained transitional region. Although the film crystal structure and stoichiometry evolve gradually from the highly distorted pseudo-perovskite structure to the BFMO322 supercell through interlayers I and II (Figs. 4 and 6), no strain gradient was found in either interlayer, i.e., both interlayers I and II are highly strained with coherent interfaces in between (Bragg filtered images in Figs. 4 and 6). As the interlayers grow thicker, the elastic biaxial strain builds up. Up to a thickness of only about 3–4 nm, maybe because of the large misfit from the LAO substrate, the interfacial defects consisting of misfit dislocation partials were generated to relax the mismatch strain and followed by the growth of the BFMO322 supercell. This, in general, agrees well with the Matthews-Blakeslee (MB) model of thin film heteroepitaxy.[25] The distinctive feature of the BFMO322/LAO heterointerface extending from the classic MB model is the formation of the new supercell phase. However, theoretical calculation based on the Pertsev model has predicted that new materials that cannot be grown as equilibrium single crystals are possible to grow in the form of epitaxially constrained films.[26] Experimentally, it has been found that biaxial strain can promote compositional segregation[27] and crystal symmetry transformations,[14,28] the two key ingredients for new phase formation. A recent study also reported
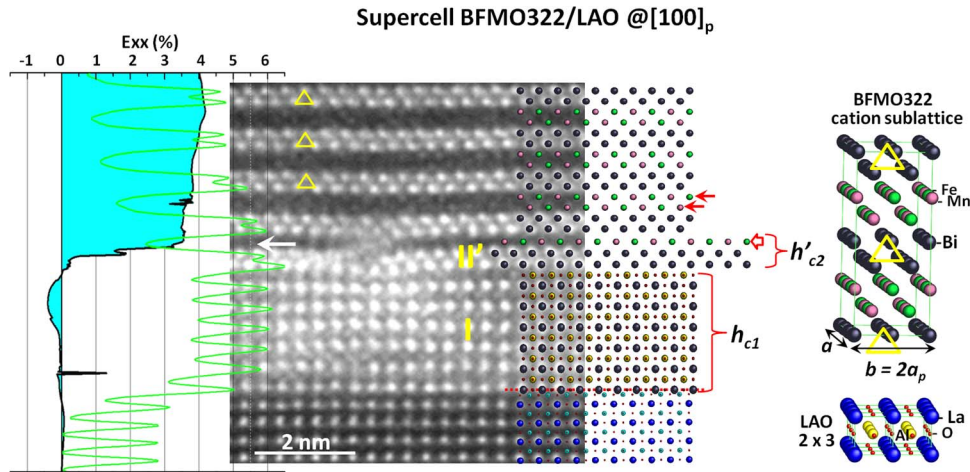
FIG. 6. Interfacial atomic contact and biaxial strain profile across the supercell BFMO322/LAO heterointerface in the [100]. The strain relaxation in the ε_{xx} profile is marked by a white arrow, which is also at the position of the misfit dislocations. Ball models of the BFMO 322 cation sublattice (1 unit-cell) and the LAO pseudo-perovskite (2/3 unit-cell) near the [100] projection are presented. Compared to that of in Fig. 4, the neighboring Bi-column triangles are the same in the out-of-plane direction under this zone axis.
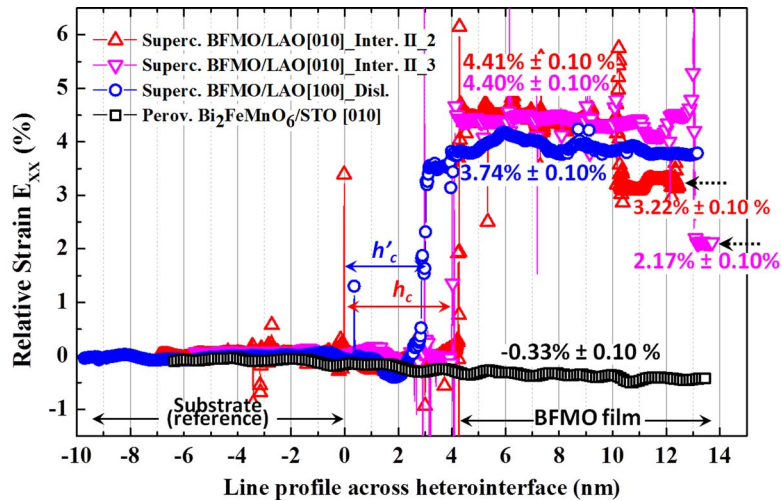

FIG. 7. A comparison of the relative biaxial strain ε_{xx} profiles across the heterointerface of the pseudo-perovskite Bi_2FeMnO_6/STO (from the strain map in Fig. 1(c)), the supercell BFMO322/LAO in [100] (Fig. 5(c)) and in [010] zone axis with the interlayer II consisting of two and three Bi_2O_2 layers (Fig. 3(c) and Fig. S1(c) of the supplementary material[19]). "0" in the x-axis of the plots is the interface between substrates and interlayer I. The black dashed arrows are corresponding to the white ones denoting the staking faults in the BFMO322 film in Fig. 3(c) and in Fig. S2(c) of the supplementary material.[19]

the observation of a transition layer with a d_c about 1 nm in a functional oxide heterostructures.[22] Thus, epitaxial growth not only produces high quality single-crystal-like films routinely, but also enables new phases in some cases.

Is biaxial lattice strain the only important factor for the formation of the new phases? To explore this question, we examined several film regions that failed to turn into the BFMO322 supercell structure. One of the representative regions with other minor film phases is presented in Fig. 8(a), obtained from the same BFMO322/LAO sample as Fig. 3. Two minor film phases, identified by Fourier transforms (FT), are the pseudo-perovskite Bi_2FeMnO_6 and the interlayer II phase. As shown in the enlarged STEM image in Fig. 8(b), after the transitional interlayer I, the BFMO film on the left adopted the pseudo-perovskite structure with an out-of-plane tilting about 1.5° clock-wise; while on the left it grows as the interlayer II phase throughout the film thickness. Similarly, we conducted GPA
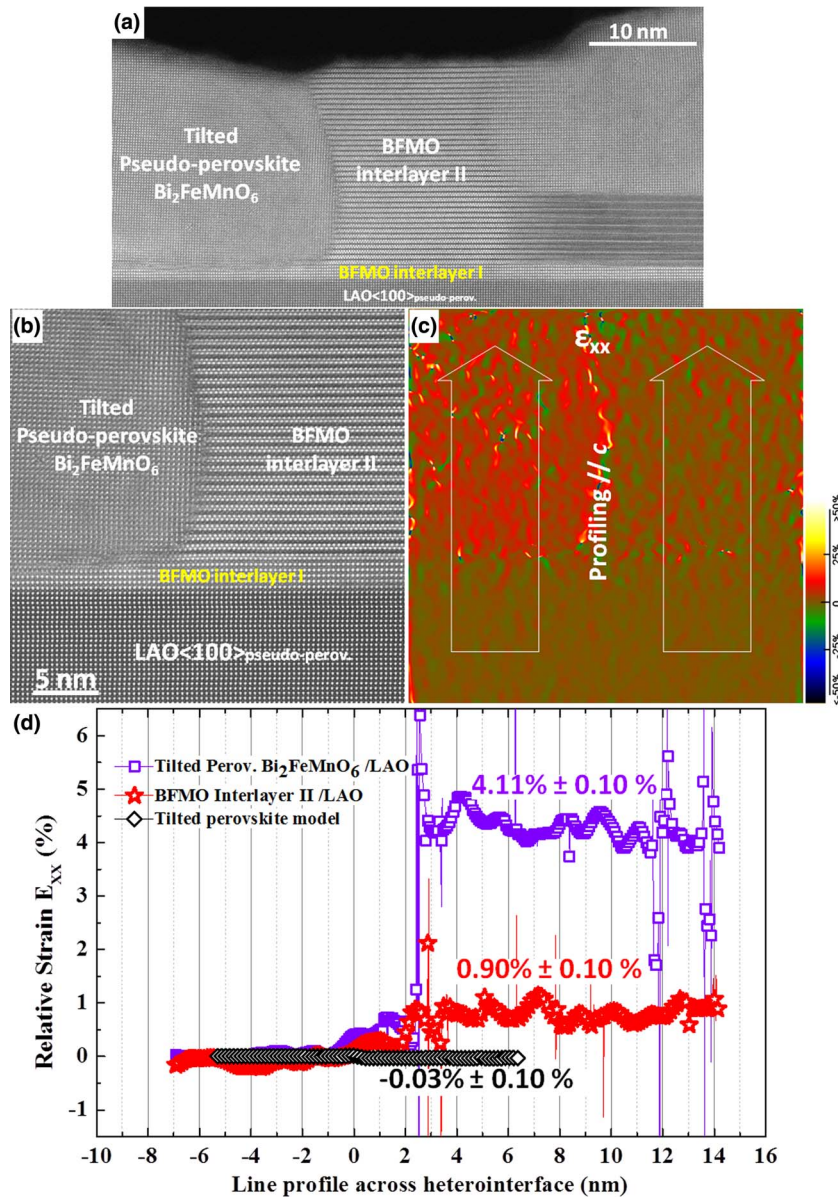
FIG. 8. (a) A STEM overview of a nanocomposite region with other minor phases in the 36 nm-thick BFMO322/LAO epitaxial thin film. (b) A STEM image of both tilted pseudo-perovskite Bi_2FeMnO_6 and the interlayer II film phases. (c) The GPA biaxial strain map ε_{xx} of (b). (d) A comparison of the relative biaxial strain ε_{xx} profiling along the two arrows in (c) and the strain profile of the tilted perovskite film model.

strain analysis and the biaxial strain profiles across the two phases in ε_{xx} strain map (Fig. 8(c)) as plotted in Fig. 8(d). Since lattice tilt can lead to lattice elongation in projection and thus lattice strain variation, this effect was proven by applying GPA on strain-free lattice model with the same 1.5° tilt (for details on the computed lattice image, please see Fig. S3 of the supplementary material).[19] It is obvious that the strain jump of 4.1% in the tilted pseudo-perovskite Bi_2FeMnO_6 region is caused by the biaxial lattice strain relaxation, rather than the tilting effect in GPA measurement (only −0.03% and with an opposite strain state). In fact, further interfacial analysis on a single-domain tilted pseudo-perovskite region revealed periodic in-plane inserting dislocations (see Fig. S4 of the supplementary material),[19] attributing to the misfit strain relaxation mechanism involving epilayer tilt.[29] It is interesting to note that the biaxial strain drops at both heterointerfaces, the BFMO322/LAO

(Fig. 7) and the tilted pseudo-perovskite Bi_2FeMnO_6 (see Fig. S4 of the supplementary material),[19] for approximately 3.5%–4.0%. However, in the latter case, the film adopted another way (a set of misfit defects) to relax the accumulated elastic misfit strain, i.e., instead of forming the BFMO322 supercell, it grows as the conventional pseudo-perovskite film. This confirms that mismatch strain is crucial for triggering new phases.

It is also surprising to see that in the right BFMO interlayer II film, a strain jump in Fig. 8(d) happened at the interface between the interlayers I and II. Although only about 0.9%, it is possible that this pre-relaxation leaves not enough elastic strain for generating additional misfit dislocations and triggering the supercell structure. It is also possible that, since the interlayer II phase is in a columnar growth (width ∼15 nm) for this case as shown in Fig. 8(a), vertical misfit strain from the neighboring film phases could also confine its lattice.[30] Then, it is probably difficult for the interlayer II to generate any planar defects providing the necessary interfacial reconstructions for the supercell BFMO322. Thus, other strain relaxation alternatives (lattice tilting, in this case) are detrimental to the new phase formation. It seems that only certain misfit defects (such as the ones in Figs. 4 and 6) reconstruct the heterointerface in a proper way that can serve as the seed pattern in favor of new phase nucleation. Furthermore, it also needs to mention that this new phase in the family of Bi-based layered structures can be reproduced routinely on LAO substrates as well as CeO_2 buffered STO and others. This again suggests that the surface seed pattern for the new phase nucleation is critical for triggering the new supercell structure. Our recent annular bright field (ABF) STEM study has confirmed that the BFMO322 supercell is related to the Aurivillius phases,[12] which is known for its richness in structure variations.[31] On the other hand, planar defects such as stacking faults intend to generate in layered structures associated with certain degree of in-plane lattice shifting. Some of these planar defects hardly affect the interfacial biaxial strain, for example, the one at the heterointerface of the pseudo-perovskite Bi_2FeMnO_6/STO (Fig. 2); some of them serve as misfit defects which relax strain effectively (Fig. 3(d)). Similar stacking faults were also found in the top supercell BFMO322 film, for example, in Fig. 3(c), in Fig. S2(c) of the supplementary material[19] denoted by dashed arrows, and in Fig. 7 showing locally tuning the film biaxial strain (as black dashed arrows). Note that these stacking faults are located in the transitional metal Fe-O/Mn-O planes, which consists of a double layer of FeO_6/MnO_6 octahedra.[12] It has been suggested that BO_6 octahedra rotations are closely related to epitaxial strain in perovskite thin films with possible orthorhombic or rhombohedral transformation.[32] This might explain the observed biaxial strain modification in the double FeO_6/MnO_6 octahedral plane.

In summary, in-depth Cs-corrected HAADF STEM and GPA lattice strain quantification have been applied to explore the growth mechanism of a new multiferroic Bi-based supercell phase. By comparing three related heterosystems, we found that under the same PLD deposition condition, BFMO film grown as epitaxially strained pseudo-perovskite Bi_2FeMnO_6 on slightly mismatched STO substrates; in the case of LAO substrates, providing a greater misfit of ∼−2.0%, the new BFMO322 supercell structure forms only when sufficiently high biaxial strain builds up as transition layers become thicker and is relaxed through a proper interfacial reconstruction. Although the criterion for new phase initiation is strict, the versatile nature of layered structures and planar defects provides the large structural diversity for possible new structures.

[1] J. L. Macmanus-Driscoll, S. R. Foltyn, Q. X. Jia, H. Wang, A. Serquis, L. Civale, B. Maiorov, M. E. Hawley, M. P. Maley, and D. E. Peterson, Nature Mater. **3**, 439 (2004).

[2] A. P. Chen, Z. X. Bi, C. F. Tsai, J. Lee, Q. Su, X. H. Zhang, Q. X. Jia, J. L. MacManus-Driscoll, and H. Y. Wang, Adv. Funct. Mater. **21**, 2423 (2011).

[3] A. P. Chen, Z. X. Bi, H. Hazariwala, X. H. Zhang, Q. Su, L. Chen, Q. X. Jia, J. L. MacManus-Driscoll, and H. Y. Wang, Nanotechnology **22**, 315712 (2011).

[4] N. A. Spaldin and M. Fiebig, Science **309**, 391 (2005).

[5] D. G. Schlom, L. Q. Chen, C. B. Eom, K. M. Rabe, S. K. Streiffer, and J. M. Triscone, Annu. Rev. Mater. Res. **37**, 589 (2007).

[6] A. P. Chen, Z. X. Bi, Q. X. Jia, J. L. MacManus-Driscoll, and H. Y. Wang, Acta Mater. **61**, 2783 (2013).

[7] J. Narayan and B. C. Larson, J. Appl. Phys. **93**, 278 (2003).

[8] H. Wang, S. R. Foltyn, P. N. Arendt, Q. X. Jia, J. L. MacManus-Driscoll, L. Stan, Y. Li, X. Zhang, and P. C. Dowden, J. Mater. Res. **19**, 1869 (2004).

[9] H. Z. Zeng, Y. Lin, and C. L. Chen, Integr. Ferroelectr. **125**, 73 (2011).

[10] S. J. Pennycook, H. Zhou, M. F. Chisholm, A. Y. Borisevich, M. Varela, J. Gazquez, T. J. Pennycook, and J. Narayan, Acta Mater. **61**, 2725 (2013).

[11] H. Zhou, M. F. Chisholm, T. H. Yang, S. J. Pennycook, and J. Narayan, J. Appl. Phys. **110**, 073515 (2011).

[12] A. P. Chen, H. H. Zhou, Z. X. Bi, Y. Y. Zhu, Z. P. Luo, A. Bayraktaroglu, J. Phillips, E. M. Choi, J. L. MacManus-Driscoll, S. J. Pennycook, J. Narayan, Q. X. Jia, X. H. Zhang, and H. Y. Wang, Adv. Mater. **25**, 1028 (2013).

[13] Y. Takamura, F. Yang, N. Kemik, E. Arenholz, M. D. Biegalski, and H. M. Christen, Phys. Rev. B **80**, 180417(R) (2009).

[14] E. M. Choi, S. Patnaik, E. Weal, S. L. Sahonta, G. Mecklenburg, H. Wang, Z. Bi, J. Xiong, M. G. Blamire, Q. X. Jia, and J. L. MacManus-Driscoll, Appl. Phys. Lett. **98**, 139903 (2011).

[15] Y. Zhu, C. Ophus, J. Ciston, and H. Wang, Acta Mater. **61**, 5646 (2013).

[16] U. Dahmen, R. Erni, V. Radmilovic, C. Kisielowski, M. D. Rossell, and P. Denes, Philos. Trans. R. Soc. London, Ser. A **367**, 3795 (2009).

[17] C. Kisielowski, B. Freitag, M. Bischoff, H. van Lin, S. Lazar, G. Knippels, P. Tiemeijer, M. van der Stam, S. von Harrach, M. Stekelenburg, M. Haider, S. Uhlemann, H. Muller, P. Hartel, B. Kabius, D. Miller, I. Petrov, E. A. Olson, T. Donchev, E. A. Kenik, A. R. Lupini, J. Bentley, S. J. Pennycook, I. M. Anderson, A. M. Minor, A. K. Schmid, T. Duden, V. Radmilovic, Q. M. Ramasse, M. Watanabe, R. Erni, E. A. Stach, P. Denes, and U. Dahmen, Microsc. Microanal. **14**, 469 (2008).

[18] R. Erni, M. D. Rossell, C. Kisielowski, and U. Dahmen, Phys. Rev. Lett. **102**, 0961011 (2009).

[19] See supplementary material at http://dx.doi.org/10.1063/1.4828936 for the accuracy estimated from STEM images, the formation of in-plane dislocation, lattice tilting can vary the strain, and the periodic in-plane inserting dislocations.

[20] M. J. Hytch, E. Snoeck, and R. Kilaas, Ultramicroscopy **74**, 131 (1998).

[21] Y. Y. Zhu, C. F. Tsai, and H. Y. Wang, Supercond. Sci. Technol. **26**, 025009 (2013).

[22] M. R. Bayati, R. Molaei, R. J. Narayan, J. Narayan, H. Zhou, and S. J. Pennycook, Appl. Phys. Lett. **100**, 251606 (2012).

[23] C. J. Lu, C. Li, Y. C. Zhang, W. N. Ye, F. K. Shan, and L. H. Xia, J. Appl. Phys. **106**, 113532 (2009).

[24] Y. L. Qin, C. L. Jia, K. Urban, J. H. Hao, and X. X. Xi, J. Mater. Res. **17**, 3117 (2002).

[25] J. W. Matthews, D. C. Jackson, and A. Chambers, Thin Solid Films **26**, 129 (1975).

[26] Z. G. Ban and S. P. Alpay, Mater. Res. Soc. Symp. Proc. **718**, 233 (2002).

[27] S. Estrade, J. M. Rebled, J. Arbiol, F. Peiro, I. C. Infante, G. Herranz, F. Sanchez, J. Fontcuberta, R. Cordoba, B. G. Mendis, and A. L. Bleloch, Appl. Phys. Lett. **95**, 072507 (2009).

[28] Y. L. Qin, H. W. Zandbergen, Z. Q. Yang, and J. Aarts, Philos. Mag. **85**, 4465 (2005).

[29] F. Riesz, Vacuum **46**, 1021 (1995).

[30] Y. Y. Zhu, C. F. Tsai, J. Wang, J. H. Kwon, H. Y. Wang, C. V. Varanasi, J. Burke, L. Brunke, and P. N. Barnes, J. Mater. Res. **27**, 1763 (2012).

[31] P. Boullay, G. Trolliard, D. Mercurio, J. M. Perez-Mato, and L. Elcoro, J. Solid State Chem. **164**, 252 (2002).

[32] A. Vailionis, H. Boschker, W. Siemons, E. P. Houwman, D. H. A. Blank, G. Rijnders, and G. Koster, Phys. Rev. B **83**, 064101 (2011).